

Kinetic and chemical characterization of aldehyde oxidation by fungal aryl-alcohol oxidase

Patricia FERREIRA*†, Aitor HERNÁNDEZ-ORTEGA*, Beatriz HERGUEDAS†, Jorge RENCORET‡¹, Ana GUTIÉRREZ‡, María Jesús MARTÍNEZ*, Jesús JIMÉNEZ-BARBERO*, Milagros MEDINA†² and Ángel T. MARTÍNEZ*²

*Centro de Investigaciones Biológicas (CIB), Consejo Superior de Investigaciones Científicas (CSIC), Ramiro de Maeztu 9, E-28040 Madrid, Spain, †Departamento de Bioquímica y Biología Molecular y Celular, Facultad de Ciencias, and Instituto de Biocomputación y Física de Sistemas Complejos, Universidad de Zaragoza, E-50009 Zaragoza, Spain, and ‡Instituto de Recursos Naturales y Agrobiología de Sevilla (IRNAS), Consejo Superior de Investigaciones Científicas (CSIC), PO Box 1052, E-41080 Seville, Spain

Fungal AAO (aryl-alcohol oxidase) provides H_2O_2 for lignin biodegradation. AAO is active on benzyl alcohols that are oxidized to aldehydes. However, during oxidation of some alcohols, AAO forms more than a stoichiometric number of H_2O_2 molecules with respect to the amount of aldehyde detected due to a double reaction that involves aryl-aldehyde oxidase activity. The latter reaction was investigated using different benzylic aldehydes, whose oxidation to acids was demonstrated by GC-MS. The steady- and presteady state kinetic constants, together with the chromatographic results, revealed that the presence of substrate electron-withdrawing or electron-donating substituents had a strong influence on activity; the highest activity was with *p*-nitrobenzaldehyde and halogenated aldehydes and the lowest with methoxylated aldehydes. Moreover, activity was correlated to the aldehyde hydration rates estimated by 1H -NMR. These findings, together with the absence in the AAO active site of a residue able to drive oxidation via an aldehyde thiohemiacetal,

suggested that oxidation mainly proceeds via the *gem*-diol species. The reaction mechanism (with a solvent isotope effect, $^2H_2O k_{red}$, of approx. 1.5) would be analogous to that described for alcohols, the reductive half-reaction involving concerted hydride transfer from the α -carbon and proton abstraction from one of the *gem*-diol hydroxy groups by a base. The existence of two steps of opposite polar requirements (hydration and hydride transfer) explains some aspects of aldehyde oxidation by AAO. Site-directed mutagenesis identified two histidine residues strongly involved in *gem*-diol oxidation and, unexpectedly, suggested that an active-site tyrosine residue could facilitate the oxidation of some aldehydes that show no detectable hydration. Double alcohol and aldehyde oxidase activities of AAO would contribute to H_2O_2 supply by the enzyme.

Key words: aromatic aldehyde, aryl-alcohol oxidase (AAO), enzyme kinetics, *gem*-diol, GC-MS, 1H -NMR.

INTRODUCTION

Lignin removal is a central process for recycling of the carbon fixed by photosynthesis in land ecosystems. Lignin protects plant polysaccharides against microbial attack and also represents a central issue in industrial utilization of lignocellulosic biomass for the production of renewable materials, chemicals and fuels in future lignocellulose biorefineries [1]. High redox-potential peroxidases are characteristic of ligninolytic basidiomycetes (they are called white-rot fungi due to the colour of delignified wood) as recently confirmed by the comparison of fungal genomes [2,3]. Analysis of the white-rot fungal genomes available currently, including those of *Phanerochaete chrysosporium* and *Pleurotus ostreatus*, also confirmed the presence of genes encoding different types of oxidases that are responsible for providing the extracellular H_2O_2 required for lignin biodegradation as the peroxidase-oxidizing substrate. These include, among others, glyoxal oxidase (EC 1.2.3.5) first reported in *P. chrysosporium*, and AAO (aryl-alcohol oxidase; EC 1.1.3.7) mainly investigated in *Pleurotus* species [4,5].

Basidiomycetes also produce a variety of extracellular aromatic metabolites that have several roles in lignin degradation [6], and are also of interest for the flavour and fine-chemical industry, as in the case of aromatic aldehydes [7]. Veratryl alcohol is synthesized by *P. chrysosporium*, where it acts as a lignin-peroxidase redox mediator, whereas the *Pleurotus* versatile peroxidase does not

require such a mediator [8]. Therefore, in *Pleurotus* species, the most abundant extracellular metabolite is *p*-anisaldehyde, together with its corresponding acid and alcohol, and some chlorinated metabolites (such as 3-chloro-*p*-anisaldehyde), with veratryl alcohol being found only in low levels [9]. It has been shown that the above anisyl compounds are redox-cycled, with the participation of AAO and mycelial dehydrogenases, resulting in the continuous generation of extracellular H_2O_2 for lignin biodegradation at the expense of intracellular reducing power [9,10].

AAO is an extracellular FAD-containing enzyme in the GMC (glucose-methanol-choline) oxidoreductase family. It catalyses the oxidative dehydrogenation of a variety of aromatic (and some aliphatic polyunsaturated) alcohols with an α -carbon primary hydroxy group, with the concomitant reduction of O_2 to H_2O_2 (Figure 1A), but it has also been suggested that it has the ability to oxidize aromatic aldehydes [11,12]. AAO was cloned for the first time in *P. eryngii* and, after that, has been expressed in *Emerella nidulans* (conidial state, *Aspergillus nidulans*) and *Escherichia coli* for further characterization of the enzyme and its alcohol oxidation mechanism [13–17]. However, to date the aldehyde reaction of AAO has remained basically unstudied.

In the present work we provide the first characterization of aldehyde oxidation by AAO using steady- and pre-steady state kinetics of wild-type AAO and some mutated variants. The kinetic studies have been accompanied by GC-MS and NMR analyses

Abbreviations used: AAO, aryl-alcohol oxidase; HRP, horseradish peroxidase; AAO_{ox}, oxidized AAO; AAO_{red}, reduced AAO.

¹ Present address: Great Lakes Bioenergy Research Center, University of Wisconsin-Madison, Madison, WI, U.S.A.

² Correspondence may be addressed to either of these authors (email mmedina@unizar.es or atmartinez@cib.csic.es)

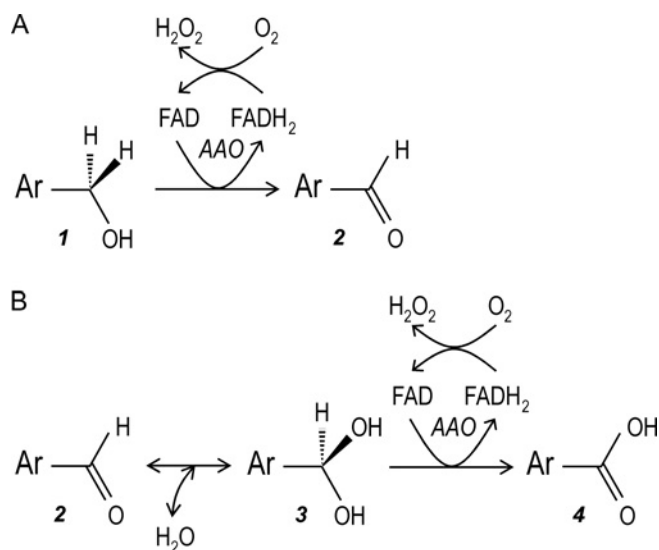


Figure 1 Scheme for reactions catalysed by AAO

(A) In the reductive half-reaction, AAO typically oxidizes aromatic alcohols (**1**) to the corresponding aldehydes (**2**) [11,17]. (B) However, it has been found that the enzyme can also oxidize aromatic aldehydes (**2**) to the corresponding acids (**4**). It is proposed that the second reaction mainly proceeds via the *gem*-diols (**3**) formed by aldehyde hydration. In both cases, H₂O₂ is generated by O₂ reduction during FAD regeneration (oxidative half-reaction). Under natural conditions H₂O₂ is continuously generated by AAO in the redox cycling of benzylic fungal metabolites (alcohols, aldehydes and acids), also involving mycelial dehydrogenases [10,39]. Ar, aromatic.

of substrates and products to obtain insights into the reaction mechanism of the enzyme.

EXPERIMENTAL

Chemicals and commercial enzymes

p-Anisyl, veratryl, *m*- and *p*-chlorobenzyl, 3-chloro-*p*-anisyl, *m*- and *p*-fluorobenzyl alcohols, 2,4-hexadien-1-ol, benzaldehyde, *p*-anisaldehyde, veratraldehyde, *m*- and *p*-chlorobenzaldehyde, 3-chloro-*p*-anisaldehyde, *m*- and *p*-fluorobenzaldehyde, 3,4-difluorobenzaldehyde, *p*-nitrobenzaldehyde, 2,4-dinitrobenzaldehyde, 2,4-hexadienal, and benzoic, *p*-anisic, veratric, *m*-chlorobenzoic, 3-chloro-*p*-anisic, and *m*- and *p*-nitrobenzoic acids were obtained from Sigma–Aldrich. Glucose oxidase (from *A. niger*; type II) and aldehyde dehydrogenase (from *Saccharomyces cerevisiae*) were also obtained from Sigma–Aldrich. Amplex[®] Red was from Invitrogen. HRP (horseradish peroxidase) was from Roche. 5-Deazariboflavin was a gift from Dr G. Tollin (University of Arizona, Tucson, AZ, U.S.A.).

AAO production

Recombinant AAO from *P. eryngii* was obtained by *E. coli* expression of the mature AAO cDNA (GenBank[®] accession number AF064069) followed by *in vitro* activation and purification as described previously [14]. AAO concentrations were determined using the molar absorption coefficient ($\epsilon_{463} = 11050 \text{ M}^{-1} \cdot \text{cm}^{-1}$).

In addition to the above wild-type AAO, H502S, H546S and Y92F variants were prepared by PCR using the QuikChange site-directed mutagenesis kit (Stratagene). The cDNA of AAO cloned into the pFLAG1 vector (International Biotechno-

logies) was used as template and the following oligonucleotides, including mutations (underlined text) at the corresponding triplets (bold text), were used as primers (only direct constructions are shown): Y92F, 5'-GGTCTAGCTCT-GTTCACTTTCATGGTCATGATGCG-3'; H502S, 5'-GCCAAC-ACGATTTTCAGCCAGTTGGAACGGCC-3'; and H546S, 5'-CCCTTCGCGCCCAACGCAAGTACCCAAGGACCG-3'. The mutant plasmids were isolated and AAO cDNA was sequenced (GS-FLX sequencer from Roche) to confirm that only the designed mutations were introduced. The variants were produced as indicated above for wild-type AAO.

Steady-state studies

Steady-state kinetic constants for AAO aldehyde oxidation were calculated by monitoring H₂O₂ production using an HRP-coupled assay with Amplex[®] Red at 24 °C in air-saturated 0.1 M sodium phosphate buffer, pH 6. Turnover reactions were initiated by addition of AAO with an adder-mixer. In the presence of the H₂O₂ generated by AAO, HRP (6 units/ml) oxidizes Amplex[®] Red (60 μM) forming resorufin ($\epsilon_{563} = 52000 \text{ M}^{-1} \cdot \text{cm}^{-1}$) [18]. After non-linear fitting of data (three replicates) using SigmaPlot, mean and standard errors were obtained from the normalized Michaelis–Menten equation. *p*-Nitrobenzaldehyde (7 mM) oxidation by the H502S and H546S AAO variants and wild-type AAO were also estimated (as turnover numbers).

Oxidation rates of several alcohols by AAO were monitored both by aldehyde formation, using the molar absorbance coefficients [19], and by H₂O₂ generation, using an HRP-coupled assay with *o*-dianisidine, at 24 °C in air-saturated 0.1 M sodium phosphate buffer, pH 6. Assays were initiated by addition of AAO, and formation of the *o*-dianisidine oxidation product was monitored ($\epsilon_{460} 6765 \text{ M}^{-1} \cdot \text{cm}^{-1}$) [20]. The results are presented as turnover rates (k_{cat} in s⁻¹) obtained as described above.

The enzymatic activity of commercial yeast aldehyde dehydrogenase on benzaldehyde, *p*-anisaldehyde and 4-nitrobenzaldehyde was measured at 25 °C in 0.1 M Tris/HCl, pH 8.0, containing 1 M KCl and 1 mM EDTA, by following the formation of NADH ($\epsilon_{340} = 6220 \text{ M}^{-1} \cdot \text{cm}^{-1}$) from 5 mM NAD⁺.

GC-MS studies

For analysing the reaction products, 4 mM aldehyde solutions (1 mM in the cases of *p*-anisaldehyde and 3-chloro-*p*-anisaldehyde due to solubility constraints) were incubated with 0.3 μM AAO in 0.1 M sodium phosphate buffer, pH 6. After 3 h at 24 °C, under shaking, the reaction mixtures were acidified (pH 2–3) and liquid–liquid extracted with methyl *t*-butyl ether. Extracts were dried by evaporation and redissolved in chloroform. GC-MS analyses were performed directly, or after silylation with BSTFA [bis(trimethylsilyl)trifluoroacetamide] in the presence of pyridine. A Varian Star 3400 chromatograph equipped with a DB-5HT column (30 m \times 0.25 mm internal diameter; 0.1 μm film thickness) and coupled to an ion-trap detector (Varian Saturn 2000) was used. The oven was programmed to increase from 50 °C to 330 °C at 6 °C \cdot min⁻¹, and was held for 3 min. Both the temperature of the injector and the transfer line were 300 °C. Helium was used as the carrier gas at a flow rate of 2 ml/min. Compounds were identified by comparing their mass spectra with standards, which were also used to obtain response factors.

NMR spectroscopy

The hydration rates of aldehyde solutions ($\sim 10 \mu\text{M}$) in 0.1 M sodium phosphate buffer, pH 6, prepared with ²H₂O (isotopic

purity 99.9 %) was estimated by $^1\text{H-NMR}$ using a Bruker Avance 500 MHz instrument. The signal of residual water proton (δ_{H} 4.701 p.p.m.) was used as internal reference for chemical shifts. For the hydration rate estimation, the signal of the H-C-(OH)_2 proton in the *gem*-diol species was integrated and referred to that of the H-C=O proton of the aldehyde species. Spectra in DMSO (isotopic purity > 99.8 %) were run as a reference, showing only the non-hydrated aldehyde.

Stopped-flow measurements

Stopped-flow experiments were carried out on an Applied Photophysics SX17.MV spectrophotometer interfaced with an Acorn computer using the SX18.MV and Xscan software (from Applied Photophysics). Enzyme-monitored turnover experiments [21], as well as analysis of the reductive half-reactions under anaerobic conditions, were performed as described previously [17] in 0.1 M sodium phosphate buffer, pH 6, at 24 °C. Deconvolution of spectral data was performed by global analysis and numerical integration methods using the Pro-K software (Applied Photophysics).

For accurate estimation of observed rate constants (k_{obs}) kinetic traces were recorded at 462 nm. These traces were fitted to the standard double-exponential or mono-exponential decays. k_{obs1} and k_{obs2} are the observed rate constants for the fast and slow phases of the reduction of the enzyme respectively. The k_{obs} values at different substrate concentrations were fitted to either eqn (1) or eqn (2):

$$k_{\text{obs}} = \frac{k_{\text{red}}A}{K_d + A} \quad (1)$$

$$K_{\text{obs}} = \frac{k_{\text{red}}A}{K_d + A} + k_{\text{rev}} \quad (2)$$

where K_d is the dissociation constant for the enzyme–substrate complex, and k_{red} and k_{rev} are the limiting rate and reverse rate of flavin reduction.

The solvent isotope effect in the reductive half-reaction of AAO with *p*-nitrobenzaldehyde was determined by measuring the rate constants using H_2O and $^2\text{H}_2\text{O}$. For assays in deuterated solvent, the reaction components were dissolved in deuterated 0.1 M sodium phosphate buffer, $p^2\text{H}$ 6. AAO was exhaustively dialysed against the deuterated buffer to remove all exchangeable protons.

Spectral characterization of AAO–acid complexes

Binding of aromatic acids was studied in 0.1 M sodium phosphate buffer, pH 6. The dissociation constants (K_d) for the complex of AAO with *p*-anisic acid and 3-chloro-*p*-anisic acid were determined from the absorption spectra during enzyme titration using eqn (3) for a 1:1 stoichiometry:

$$\Delta Abs = \frac{\Delta \epsilon(E + L + K_d) - \Delta \epsilon \sqrt{(E + L + K_d)^2 - 4EL}}{2} \quad (3)$$

where ΔAbs is the absorbance difference values, E and L are the enzyme and ligand concentration respectively, and K_d is the dissociation constant [22]. Finally, the complex of reduced AAO with *p*-anisic acid was prepared by photoreduction in the presence of EDTA and 5-deazariboflavin, as described previously [23].

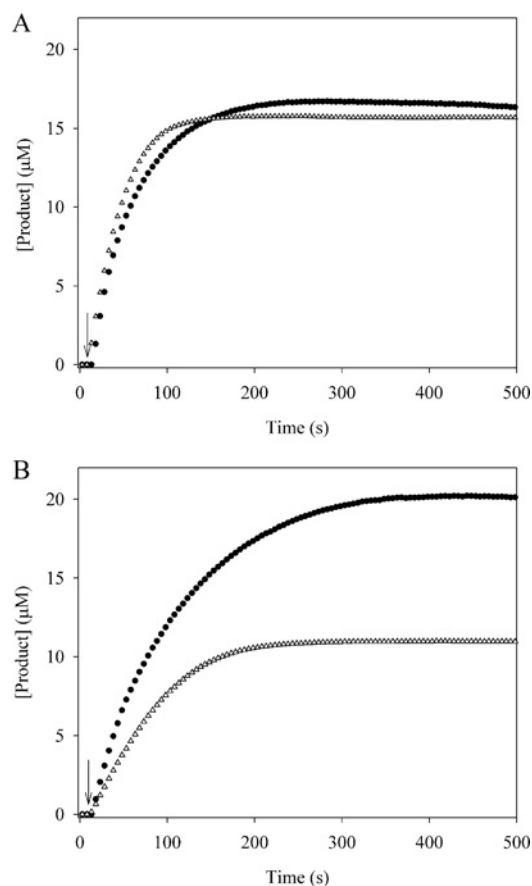


Figure 2 Aldehyde and H_2O_2 produced during AAO oxidation of *p*-anisyl and 3-chloro-*p*-anisyl alcohols

(A) *p*-Anisyl and (B) 3-chloro-*p*-anisyl (16 μM) were incubated with 0.01 μM AAO for 500 s and the concentrations of the reductive and oxidative half-reaction products were estimated spectrophotometrically (aldehyde maxima at 295 and 285 nm for 3-chloro-*p*-anisaldehyde and *p*-anisaldehyde respectively) and by the coupled H_2O_2 -dependent oxidation of Amplex[®] Red by HRP. The arrows indicate the addition of enzyme. (Δ), aldehyde; (\bullet), H_2O_2 .

RESULTS

Aldehyde oxidase activity during alcohol oxidation by AAO

The ability of AAO to continue oxidizing some aldehydes was deduced from the curves of H_2O_2 and aldehyde generated during reactions with eight aromatic alcohols (Figure 2). With *p*-anisyl alcohol, the two curves were similar and the final concentrations corresponded to the initial concentration of the alcohol, in agreement with the reaction stoichiometry (Figure 1A). However, with 3-chloro-*p*-anisyl alcohol the H_2O_2 concentration was nearly double that of 3-chloro-*p*-anisaldehyde, suggesting that a fraction of the aldehyde formed was oxidized further, releasing extra H_2O_2 . Simultaneous alcohol oxidase and aldehyde oxidase activities were also observed in the reactions of AAO with other alcohols, e.g. with *m*- and *p*-fluorobenzyl alcohols (Table 1).

Steady-state kinetics with aldehydes

To characterize the aldehyde oxidase activity of AAO, a substrate specificity profile was constructed by determining apparent steady-state kinetic parameters with nine *p*- and *m*-substituted benzylic aldehydes, benzaldehyde and 2,4-hexadienal (Table 2) [the activity on 2,4-dinitrobenzaldehyde was too low (<1 % that observed with *p*-nitrobenzaldehyde) to estimate kinetic constants (its water solubility was also low)]. Considering the AAO

Table 1 H₂O₂ and aldehyde production in AAO oxidation of different alcohols

The reactions were performed in 0.1 M sodium phosphate buffer, pH 6, at 24 °C. Results are given as turnover numbers (indicating mols of product formed by mol of enzyme in 1 s) and are means \pm S.E.M. for three replicates.

Alcohol	H ₂ O ₂ (s ⁻¹)	Aldehyde (s ⁻¹)
<i>p</i> -Anisyl alcohol	106 \pm 5	113 \pm 2
Veratryl alcohol	75 \pm 2	88 \pm 1
<i>m</i> -Chlorobenzyl alcohol	21 \pm 1	21 \pm 1
<i>p</i> -Chlorobenzyl alcohol	37 \pm 1	33 \pm 1
3-Chloro- <i>p</i> -anisyl alcohol	60 \pm 1	39 \pm 1
<i>m</i> -Fluorobenzyl alcohol	22 \pm 1	15 \pm 1
<i>p</i> -Fluorobenzyl alcohol	28 \pm 1	20 \pm 1
2,4-Hexadien-1-ol	138 \pm 2	135 \pm 2

efficiency values, *m*-chlorobenzaldehyde was the best aldehyde substrate, whereas veratraldehyde was the worst substrate. AAO showed the highest *k*_{cat} on *p*-nitrobenzaldehyde, whereas the three methoxylated benzaldehydes showed the lowest *k*_{cat} values. Despite its low activity, AAO showed the highest affinity for *p*-anisaldehyde and 3-chloro-*p*-anisaldehyde.

Aldehyde oxidation was also investigated for three AAO variants obtained by site-directed mutagenesis of two histidine

Table 3 Steady-state kinetic constants for oxidation of two aldehydes by the Y92F AAO variant and wild-type AAO

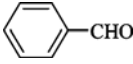


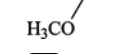
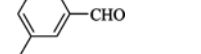
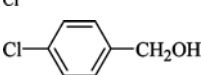
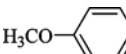
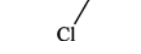
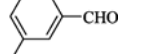
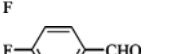
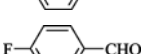
The Y92F kinetic constants were obtained as those for wild-type AAO (Table 2).

Aldehyde	<i>K</i> _m (mM)	<i>k</i> _{cat} (min ⁻¹)	<i>k</i> _{cat} / <i>K</i> _m (min ⁻¹ · mM ⁻¹)
<i>p</i> -Anisaldehyde			
Y92F	0.8 \pm 0.1	0.7 \pm 0.02	0.8 \pm 0.03
Wild-type	0.7 \pm 0.1	3.0 \pm 0.1	5.2 \pm 0.4
<i>p</i> -Nitrobenzaldehyde			
Y92F	2.0 \pm 0.3	72.6 \pm 4.3	35.8 \pm 3.7
Wild-type	5.0 \pm 0.2	98.0 \pm 2.0	18.9 \pm 0.4

residues (His⁵⁰² and His⁵⁴⁶) and one tyrosine (Tyr⁹²) residue, which are conserved in the active sites of AAO and glucose oxidase [12]. The two histidine residues seemed to be crucial for AAO oxidation of aldehydes, as the activities of the H502S and H546S variants on saturating concentrations of *p*-nitrobenzaldehyde were 0.22 \pm 0.02 min⁻¹ and 0.11 \pm 0.01 min⁻¹ respectively, compared with activity of 75.00 \pm 0.16 min⁻¹ with the wild-type enzyme (their low activities prevented estimation of kinetic constants). On the other hand, removal of the phenolic hydroxy group of Tyr⁹² had distinctive effects on the oxidation of *p*-anisaldehyde and *p*-nitrobenzaldehyde (Table 3).

Table 2 Steady-state kinetic constants for AAO oxidation of different aldehydes

Oxidation assays on a variety of aldehyde substrates were performed in 0.1 M sodium phosphate buffer, pH 6, at 24 °C. The kinetics parameters were calculated by measuring H₂O₂ production using an HRP-coupled assay. After non-linear fitting of data, means and standard errors were obtained from the normalized Michaelis–Menten equation.

Aldehyde	Structure	<i>K</i> _m (mM)	<i>k</i> _{cat} (min ⁻¹)	<i>k</i> _{cat} / <i>K</i> _m (min ⁻¹ · mM ⁻¹)
Benzaldehyde		7.0 \pm 0.8	30 \pm 1	4.4 \pm 0.4
<i>p</i> -Anisaldehyde		0.7 \pm 0.1	3.0 \pm 0.1	5.2 \pm 0.4
Veratraldehyde		8.0 \pm 1.0	8.0 \pm 0.6	1.0 \pm 0.1
<i>m</i> -Chlorobenzaldehyde		1.5 \pm 0.1	51 \pm 1	38.6 \pm 3.0
<i>p</i> -Chlorobenzaldehyde		4.7 \pm 0.3	63 \pm 1	13.4 \pm 0.5
3-Chloro- <i>p</i> -anisaldehyde		0.7 \pm 0.1	3.4 \pm 0.1	5.1 \pm 0.4
<i>m</i> -Fluorobenzaldehyde		2.2 \pm 0.2	53 \pm 1	24.4 \pm 1.4
<i>p</i> -Fluorobenzaldehyde		4.9 \pm 0.2	22.0 \pm 0.4	4.5 \pm 0.1
3,4-Difluorobenzaldehyde		3.0 \pm 0.2	52 \pm 1	16.9 \pm 0.7
<i>p</i> -Nitrobenzaldehyde		5.0 \pm 0.2	98 \pm 2	18.9 \pm 0.4
2,4-Hexadienal		13.0 \pm 2.0	20 \pm 1	1.5 \pm 0.1

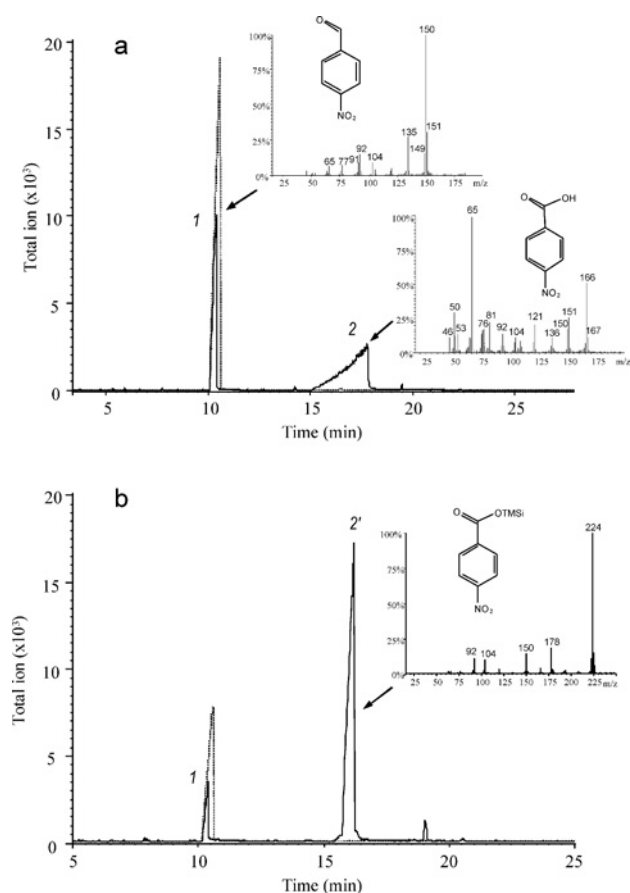


Figure 3 GC-MS of underivatized and silylated reactions of AAO with *p*-nitrobenzaldehyde

Chromatographic profiles (including controls, broken lines), and mass spectra of the aldehyde substrate (peak 1) and the acid product in its free and trimethylsilyl (TMS) ester forms (peaks 2 and 2' respectively). *p*-Nitrobenzaldehyde (4 mM) was incubated with AAO (0.3 μ M) in 0.1 M sodium phosphate buffer pH 6, for 3 h at 24 °C. The reaction mixture, and the corresponding control without enzyme, were extracted and analysed by GC-MS (a) before and (b) after silylation. The mass spectra were obtained with an ion-trap detector. The small peak with retention time around 19 min in (b) could be a dimeric reaction product. Silylation resulted in sharper acid peaks due to formation of more volatile ester derivatives. However, the recovery of the different acids was higher when the samples were analysed directly, most probably because of incomplete derivatization or side reactions in some cases.

GC-MS identification of products from aldehyde oxidase activity

The reactions products of 12 aldehydes with AAO were analysed by GC-MS directly and after silylation, as shown in Figure 3 for the *p*-nitrobenzaldehyde reaction. The mass spectra of the product peaks revealed formation of *p*-nitrobenzoic acid by AAO. The corresponding acids were also found in the reactions of AAO with most of the aldehydes (see Supplementary Table S1 available at <http://www.BiochemJ.org/bj/425/bj4250585add.htm> for the characteristic MS fragments and the quantification of the acids formed). Under the reaction conditions used, the highest oxidation rates were obtained for *p*-chlorobenzaldehyde (48 %), *p*-nitrobenzaldehyde (43 %) and *m*-chlorobenzaldehyde (39 %), followed by *p*-fluorobenzaldehyde (20 %) and *p*-anisaldehyde (17 %), no acids were detected from veratraldehyde and 2,4-dinitrobenzaldehyde and low oxidation rates (<7 %) were obtained after incubation of AAO and the other five aldehydes.

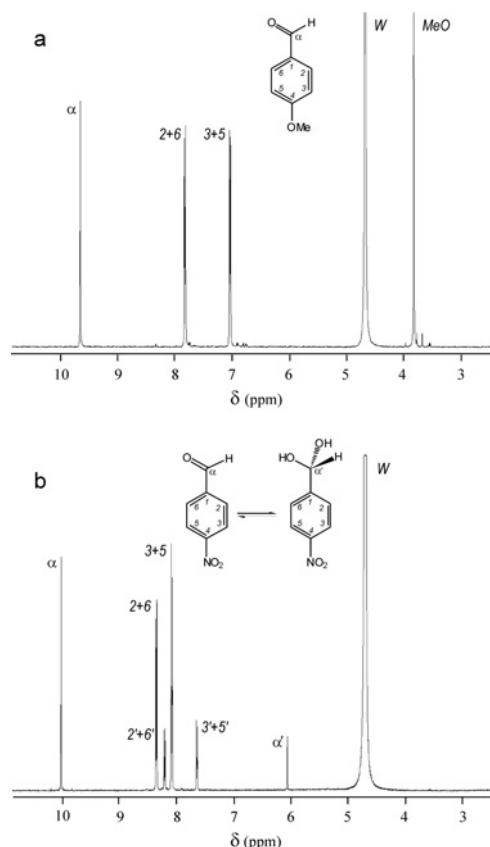


Figure 4 NMR analysis of *p*-anisaldehyde and *p*-nitrobenzaldehyde hydration

(a) *p*-Anisaldehyde and (b) *p*-nitrobenzaldehyde solutions in 0.1 M sodium phosphate buffer, pH 6 (prepared with $^2\text{H}_2\text{O}$), were analysed by ^1H -NMR yielding signals corresponding to: H_α in the aldehyde (α) and *gem*-diol (α'); $\text{H}_{2,6}$ in the aldehyde (2+6) and *gem*-diol (2'+6'); $\text{H}_{3,5}$ in the aldehyde (3+5) and *gem*-diol (3'+5'); and H_{MeO} (MeO). To estimate the hydration rate the α' signal of the *gem*-diol was integrated and referred to the α signal of the aldehyde. Similar results were obtained by referring the signals of aromatic protons in the *gem*-diol forms (2'+6' or 3'+5) to those of the corresponding protons in the aldehyde forms (2+6 or 3+5 respectively).

NMR analysis of the *gem*-diol forms of the aldehyde substrates

To investigate the possible involvement of the *gem*-diol species in aldehyde oxidation, the hydration rates of the 12 aldehydes used as AAO substrates were estimated from their ^1H -NMR spectra (Figure 4). The *p*-anisaldehyde spectrum showed only four signals (plus the residual water signal) corresponding to the methoxy, *ortho* (H_{2+6}), *meta* (H_{3+5}) and aldehyde (H_α) protons. The absence of the *gem*-diol benzylic proton signal (δ_{H} 6 p.p.m.) indicated that *p*-anisaldehyde was not hydrated. On the other hand, the *p*-nitrobenzaldehyde spectrum included the *gem*-diol signal ($\text{H}_{\alpha'}$) together with that of the aldehyde form (H_α), as well as double signals for the ring protons for both the *gem*-diol ($\text{H}_{2'+6'}$ and $\text{H}_{3'+5'}$) and the aldehyde (H_{2+6} and H_{3+5}) species, revealing partial hydration. Similar *gem*-diol signals were detected in all the other NMR spectra, with the exception of *p*-anisaldehyde and veratraldehyde, and the hydration rates were obtained by integrating the benzylic proton ($\text{H}_{\alpha'}$ and H_α) signals (the chemical shifts and the hydration rates obtained are shown in Supplementary Table S2 available at <http://www.BiochemJ.org/bj/425/bj4250585add.htm>).

The hydration rates of all the aldehydes assayed were relatively modest, with the only exception being 2,4-dinitrobenzaldehyde.

The highest values were obtained for the aromatic aldehydes bearing electron-withdrawing substituents, which facilitated the hydration reaction when located at the *ortho* or *para* positions, such as one or two nitro groups (20 % and 83 % hydration respectively), or at the *meta* position, such as chlorine (4 %) or fluorine (3 %) atoms. The presence of halogen atoms at the *para* position did not increase hydration with respect to benzaldehyde (1 %), as expected from the above mentioned *meta* orientation of their electron-withdrawing effect, and the same was observed when comparing the hydration rates of 3,4-difluorobenzaldehyde and *m*-fluorobenzaldehyde (both being 3 %). In contrast, the presence of methoxy substituents, acting as electron donors, especially at the *para* position, resulted in the complete absence of the *gem*-diol form, as found for *p*-anisaldehyde and veratraldehyde. Finally, the aliphatic polyunsaturated 2,4-hexadienal showed a very low hydration rate (below 1 %).

Oxidation of benzylic aldehydes by yeast aldehyde dehydrogenase

The possible influence of different ring substituents on aromatic aldehyde oxidation by yeast aldehyde dehydrogenase, which does not oxidize the *gem*-diol forms, but acts on the non-hydrated aldehydes, was investigated. Interestingly, although the catalytic efficiency of aldehyde dehydrogenase oxidizing benzaldehyde was higher than on *p*-anisaldehyde, it was not increased further by the presence of an electron-withdrawing substituent in *p*-nitrobenzaldehyde (see Supplementary Figure S1 available at <http://www.BiochemJ.org/bj/425/bj4250585add.htm>) as found with AAO.

Stopped-flow spectrophotometric studies

By monitoring the redox state of the cofactor during AAO catalysis, information was obtained about the rate-limiting step. Using *p*-nitrobenzaldehyde as substrate, it was found that the enzyme is fully oxidized under air-saturated steady-state conditions (Figure 5). This corresponded to the first 1–2 min of the reaction (Figure 5, inset) when O₂ availability is not a limiting factor, and this indicated that the reductive half-reaction by the aldehyde is much slower than the oxidative half-reaction by O₂.

Pre-steady-state reduction of the oxidized enzyme by *p*-anisaldehyde, 3-chloro-*p*-anisaldehyde, veratraldehyde and *p*-nitrobenzaldehyde was investigated under anaerobic conditions (Figure 6, and Supplementary Figure S2 available at <http://www.BiochemJ.org/bj/425/bj4250585add.htm>). The first spectra, obtained after mixing AAO with the different aldehydes were in general different from those observed in the absence of substrate (Figure 6), showing displacement of the main flavin band (462 nm) and increased absorbance. These changes reflected formation of the oxidized enzyme complex with the aldehyde substrate (AAO_{ox}-S). The subsequent decrease at 462 nm corresponded to the reductive half-reaction. Formation of a charge-transfer complex between the reduced enzyme and the product (AAO_{red}-P), characterized by a peak at 490 nm and a long-wavelength band, was also observed in the *p*-anisaldehyde reaction (Figure 6a), and the 3-chloro-*p*-anisaldehyde and veratraldehyde reactions (Supplementary Figure S2). The spectral course of the reductive half-reaction fitted to an irreversible two-step process without formation of any intermediate species for *p*-anisaldehyde, 3-chloro-*p*-anisaldehyde and veratraldehyde (with rate constants at saturating substrate concentrations of 1.32, 0.76 and 0.18 min⁻¹ respectively) (Figure 6a and Supplementary Figure S2). However, AAO reduction by *p*-nitrobenzaldehyde best fitted a three-step process (Figure 6b), its initial phase being considerably faster (a rate constant over 90 min⁻¹) than the reduction by the

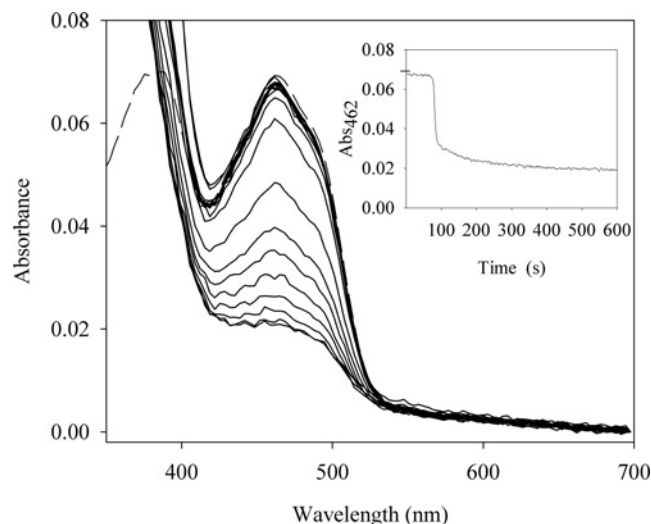


Figure 5 Spectral changes during AAO turnover with *p*-nitrobenzaldehyde showing that the reductive half-reaction was rate-limiting

An aerobic solution of 6.3 μ M AAO was mixed in the stopped-flow spectrophotometer with 2 mM *p*-nitrobenzaldehyde in 0.1 M sodium phosphate buffer, pH 6, at 24 °C, and spectra were acquired with a diode-array detector. The oxidized AAO spectrum before mixing is indicated as a broken line. Spectra recorded after 0.019, 10, 20, 30, 40, 50, 60, 70, 76, 79, 84, 87, 102, 150, 199, 300 and 400 s are shown. The inset shows the time evolution of 462 nm absorbance, revealing that the enzyme was fully oxidized under steady-state oxidation of the aldehyde.

other aldehyde substrates (Figure 6c). The dependence of k_{obs} on aldehyde concentration was determined with *p*-nitrobenzaldehyde (which showed 20 % hydration and the highest turnover) and *p*-anisaldehyde (which showed low reactivity and no detectable *gem*-diol). These k_{obs} dependencies exhibited hyperbolic saturation profiles with a good fit to eqn (1), suggesting an essentially irreversible flavin reduction and allowing the determination of transient constants for *p*-anisaldehyde (k_{red} of 1.5 ± 0.2 min⁻¹ and K_d of 0.032 ± 0.019 mM) and *p*-nitrobenzaldehyde (k_{red} of 356 ± 38 min⁻¹ and K_d of 5.79 ± 0.77 mM). In the case of *p*-nitrobenzaldehyde, AAO reduction is completed in a second slow phase (k_{red} of approx. 0.74 min⁻¹).

Using deuterated buffer, a solvent isotope effect with a $^2\text{H}_2\text{O}$ / k_{red} value of 1.5 (representing the ratio between k_{red} in H₂O and in $^2\text{H}_2\text{O}$) was observed in the fast AAO reductive half-reaction with *p*-nitrobenzaldehyde.

Spectral characterization of AAO complexes with aromatic acids

It was found that aromatic acids bind at that point that the AAO absorption spectrum is modified (as illustrated in Supplementary Figure S3a, available at <http://www.BiochemJ.org/bj/425/bj4250585add.htm>, for the AAO titration with 3-chloro-*p*-anisic acid). Qualitatively similar difference spectra were also obtained with *p*-anisic, veratric, *m*-chlorobenzoic, *m*-fluorobenzoic and benzoic acids (results not shown). The tightest binding was observed with 3-chloro-*p*-anisic acid and *p*-anisic acid resulting in K_d of 31.5 ± 0.1 μ M and 94 ± 3 μ M respectively. The low AAO affinity for the other acids suggested K_d values in the millimolar range. The spectrum of the AAO_{red}-(*p*-anisic acid) complex (Supplementary Figure S3b) was obtained by photoreduction of the AAO_{ox}-(*p*-anisic acid) complex. It was characterized by the displacement of the flavin maximum to approx. 490 nm and absorbance in the 520–600 nm region, being similar to that observed at the end of the stopped-flow experiments with *p*-anisaldehyde. This indicated that the fully reduced species

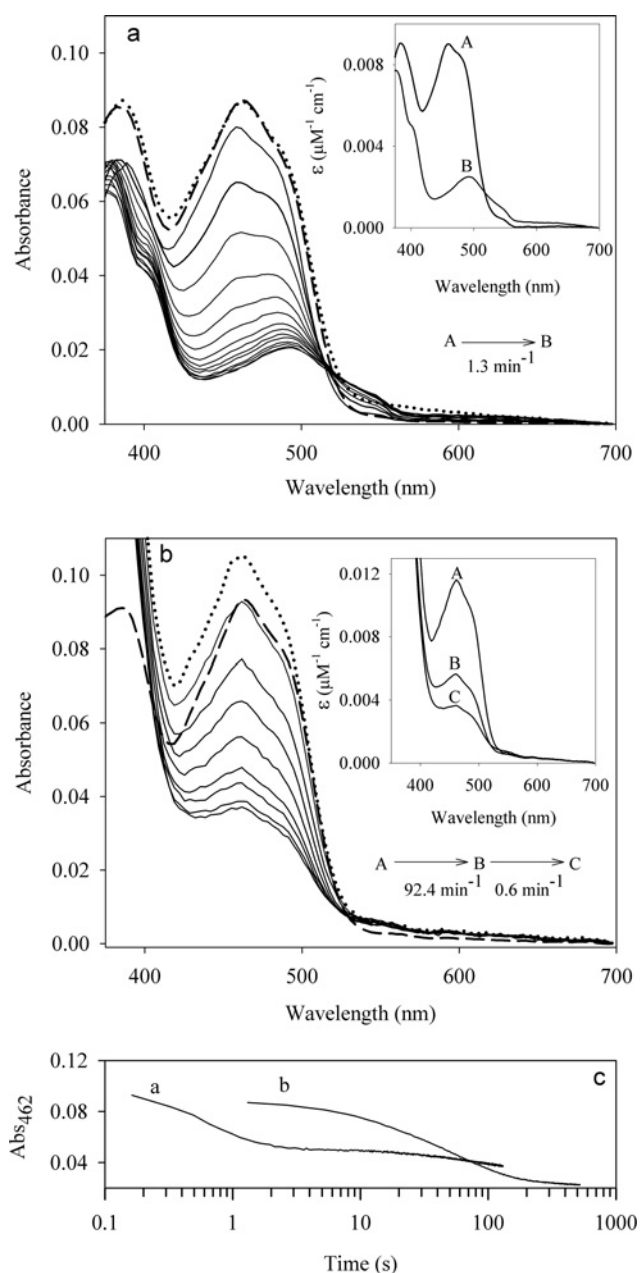


Figure 6 Spectral course of anaerobic reduction of AAO with two different aldehydes

AAO ($\sim 8 \mu\text{M}$) reduction with (a) 0.5 mM *p*-anisaldehyde and (b) 2.0 mM *p*-nitrobenzaldehyde in 0.1 M sodium phosphate buffer, pH 6, at 24°C was monitored using a diode-array stopped-flow spectrophotometer under anaerobic conditions. The initial AAO spectrum, and the first spectrum after mixing with the aldehydes are shown as (---) and (· · ·) respectively. Spectra were recorded at different times after aldehyde addition: for (a) after 0.5, 1, 13, 29, 52, 76, 102, 128, 152, 176, 202, 301, and 404 s; and for (b) after 0.009, 0.16, 0.5, 0.8, 1.5, 20, 50, 100 and 130 s. Insets show a deconvolution of the spectral changes during AAO reduction fitting to a two step model (A \rightarrow B) in (a), whereas the process in (b) is better described by a three steps model (A \rightarrow B \rightarrow C) (A, B and C are spectral species, reflecting distribution of reactants, intermediates or products, and do not necessarily represent distinct enzyme intermediates). (c) A comparison of kinetics traces at 462 nm during AAO reduction with the two aldehydes.

observed after AAO reduction with this aldehyde, as well as with 3-chloro-*p*-anisaldehyde, is the AAO_{red}-acid complex (Figures 6a and 6b). The other acids showed much looser binding and therefore no AAO_{red}-acid complexes were detected at the end of AAO reduction (Supplementary Figure S2).

DISCUSSION

Aldehyde oxidase activity of AAO: aldehyde hydration and enzymatic oxidation

AAO typically oxidizes aromatic alcohols to the corresponding aldehydes, with the concomitant production of H₂O₂ [11,19] (Figure 1A). In the present study we demonstrated the ability of the enzyme to continue the oxidation of some alcohols to the corresponding acids, in agreement with preliminary ¹⁹F-NMR results [19]. The aldehyde oxidase activity of AAO was confirmed by analysis of the mass spectra of the acids formed from a variety of aldehydes. The GC-MS results were in good agreement with the k_{cat} values obtained, *p*-nitrobenzaldehyde and two chlorobenzaldehydes appeared to be the best AAO substrates in both cases.

In water solution, carbonyl compounds exist in equilibrium with their *gem*-diol forms. The hydration rates of the aromatic aldehydes are generally low compared with the aliphatic ones, and that of benzaldehyde is often considered as negligible. However, using ¹H-NMR we demonstrated that all the aldehydes studied presented detectable hydration rates, with the exception of veratraldehyde and *p*-anisaldehyde. The rates could be correlated to the presence of electron-withdrawing or electron-donating substituents that stabilize or destabilize the *gem*-diol form.

Enzymatic oxidation of aldehydes often is catalysed using the unhydrated form, when an active-site residue forms a covalent adduct that favours oxidation. The most classical examples are aldehyde dehydrogenases, where a cysteine residue forms a thiohemiacetal linkage with the aldehyde substrate [24]. Active-site serine, glutamate or lysine residues could also activate aldehydes by forming adducts under specific conditions [25]. Alternatively, active-site metals can promote *in situ* hydration, as suggested for benzaldehyde oxidation by horse liver alcohol dehydrogenase [26] and mammalian aldehyde oxidases [27]. The structure of the AAO active site (PDB entry 3FIM) shows that no residues susceptible to forming aldehyde adducts are present, and the enzyme does not contain metals [16]. This, together with the observed correlation between the oxidation rates and the hydration of aldehydes, suggested that water is the activating molecule in aldehyde oxidation by AAO (Figure 1B). Oxidation of hydrated aldehydes has been reported for histidinol dehydrogenase [25], two mutated aldehyde dehydrogenases [28,29] and choline oxidase [30]. Moreover, a positive correlation between aldehyde hydration and oxidation rates has also been found for *Drosophila melanogaster* alcohol oxidase [31]. The similar activities obtained for benzaldehyde and *p*-nitrobenzaldehyde oxidation by yeast aldehyde dehydrogenase contrasted with those found for AAO, and supported different oxidation mechanisms by both enzymes.

The aldehyde oxidase activity of AAO is low compared with its alcohol oxidase activity [19]. However, when the variable hydration rates were taken into account, the highest activity corresponded to the *gem*-diols of *m*-fluorobenzaldehyde, *p*-fluorobenzaldehyde and *p*-chlorobenzaldehyde and their corrected k_{cat} values (100–130 s⁻¹) were close to those obtained for the best alcohol substrates of AAO [17].

Mechanisms of aldehyde oxidation by AAO

If, as suggested above, the preferred aldehyde substrates of AAO are the *gem*-diol forms, which co-exist with the carbonyl ones, the mechanism of the rate-limiting reductive half-reaction would probably be similar to that recently reported for AAO oxidation of alcohols, characterized by the concerted transfer of the

α -carbon hydride to flavin and the hydroxy proton to a catalytic base [17]. The very slow AAO oxidation of 2,4-dinitrobenzaldehyde (despite its high hydration rate) can be explained because, once hydration has been promoted by the two nitro groups, their electron-withdrawing action will make the hydride transfer difficult. A similar situation was reported for oxidation of chlorinated acetaldehyde *gem*-diols by *D. melanogaster* alcohol dehydrogenase [31].

Cleavage of one of the *gem*-diol O–H bonds would involve an active-site histidine residue acting as a base, as suggested for conserved His⁵⁰² or His⁵⁴⁶ (Supplementary Figure S4 available at <http://www.BiochemJ.org/bj/425/bj4250585add.htm>) in alcohol oxidation by AAO [32]. This was confirmed by the analysis of the H502S and H546S AAO variants, which showed much lower activities on *p*-nitrobenzaldehyde than the wild-type enzyme. The 340-fold activity decrease of H502S was in the range of that reported for *p*-anisyl alcohol oxidation [33], but that of H546S (670-fold) was higher than that reported for alcohol oxidation by over 60-fold [33], indicating that this residue plays a more important role in the AAO-mediated oxidation of *gem*-diols compared with alcohols.

A concerted cleavage of *gem*-diol C–H and O–H bonds is suggested by the solvent kinetic isotope effect for the AAO reduction by *p*-nitrobenzaldehyde ($^2\text{H}_2\text{O} k_{\text{red}} 1.5$), which was similar to that reported for its reduction by *p*-anisyl alcohol and 2,4-hexadien-1-ol [17]. The above AAO oxidation mechanism contrasts with the sequential mechanism, involving previous alcohol activation to the alkoxide without a detectable solvent isotope effect, as reported for choline oxidase [34,35].

Substitution of Tyr⁹², which is located over the AAO flavin ring (see Supplementary Figure S4), for a phenylalanine residue did not strongly affect the oxidation of *p*-nitrobenzaldehyde, in agreement with previous alcohol oxidation results [32]. However, the Y92F mutation caused a 5-fold reduction in the *p*-anisaldehyde k_{cat} value, suggesting that the phenolic hydroxy group has some effect on the activation of aldehydes that are not spontaneously hydrated. Alternatively, Tyr⁹² could promote the oxidation of a minor *gem*-diol form below the detection level of ^1H -NMR. Oxidation of small molar fractions of preformed *gem*-diol and enzyme-aided hydration have been proposed as two alternative hypotheses to explain aldehyde oxidation by some alcohol dehydrogenases [26,36] and histidinol dehydrogenase [37].

AAO is a versatile oxidase providing H₂O₂ for lignin degradation

A difference between AAO and other oxidases/dehydrogenases which catalyse oxidation of alcohols to acids concerns the eventual release of the aldehyde intermediates. As the specific reaction catalysed by choline oxidase is the conversion of choline into glycine betaine, the intermediate betaine aldehyde is not released from the enzyme under physiological conditions (although the enzyme is able to oxidize it when it is exogenously added) [38]. The same occurs in the histidinol dehydrogenase reaction [37]. In contrast, the physiological role of AAO is generation of extracellular H₂O₂, in a double-redox-cycle (alcohol \leftrightarrow aldehyde and aldehyde \leftrightarrow acid), where the oxidation products are not incorporated to metabolic pathways but reduced back by mycelium-associated dehydrogenases for the continuous supply of the peroxide required for lignin biodegradation [10,39].

Interestingly, those basidiomycetes producing AAO, typically *Pleurotus* and *Bjerkandera* species [11,40], also synthesize methoxylated and halogenated aromatic compounds, which can be detected in the extracellular medium (as alcohols, aldehydes and/or acids) [9,41]. *p*-Anisyl and 3-chloro-*p*-

anisyl compounds are among the most abundant *Pleurotus* [9] and *Bjerkandera* [42,43] metabolites. On the other hand, although few nitroaromatics are synthesized by basidiomycetes compared with the extended production of haloaromatics [44], *p*-nitrobenzaldehyde biosynthesis has been reported [45] and *p*-nitrosalicylic acid was very recently found in *Pleurotus* cultures (Giovanni Sannia, personal communication). It seems that AAO has evolved to use differently substituted benzylic metabolites for H₂O₂ production. Depending on the compound available, AAO will behave basically as an alcohol oxidase (e.g. in the presence of veratrylic and anisyl metabolites), as an aldehyde oxidase (e.g. in the presence of *p*-nitrobenzylic metabolites) or as a double-oxidase being able to transform alcohols into the corresponding acids (e.g. in the presence of 3-chloro-*p*-anisyl metabolites) (reactions shown in Figures 1A and 1B respectively). This substrate versatility would help AAO to provide a maximal supply of H₂O₂ for lignin biodegradation under variable physiological and environmental conditions.

AUTHOR CONTRIBUTION

All of the authors performed the research and discussed the results obtained. Patricia Ferreira specifically contributed with the kinetic studies and design of the enzymatic part of the study; Aitor Hernandez with the preparation and characterization of the mutated variants; Beatriz Herguedas with some spectroscopic studies; Jorge Rencoret and Ana Gutiérrez with the GC-MS analyses; Jesús Jiménez-Barbero with the NMR analyses; María Jesús Martínez in enzyme characterization; and Milagros Medina in the interpretation of the pre-steady state kinetics and other results. Angel Martínez was responsible for the co-ordination of the study.

ACKNOWLEDGEMENTS

The authors thank Antonio Romero (Centro de Investigaciones Biológicas, Consejo Superior de Investigaciones Científicas, Madrid, Spain) for providing access to the AAO crystal structure, and Vincenzo Lettera and Giovanni Sannia (University of Naples, Italy) for information on the *Pleurotus* nitroaromatic metabolites.

FUNDING

This work was supported by the Spanish Biotechnology Programme [grants numbers BIO2007-65890-C02-01, BIO2008-01533] and the Biorenew project of the European Union [grant number NMP2-CT-2006-026456]. P.F. was a recipient of a Programa Juan de la Cierva contract from the Spanish Ministry of Science and Innovation, and J.R. was a recipient of an I3P Fellowship of the Consejo Superior de Investigaciones Científicas.

REFERENCES

- Martínez, A. T., Ruiz-Dueñas, F. J., Martínez, M. J., del Río, J. C. and Gutiérrez, A. (2009) Enzymatic delignification of plant cell-wall: from nature to mill. *Curr. Opin. Biotechnol.* **20**, 348–357.
- Martínez, D., Challacombe, J., Morgenstern, I., Hibbett, D. S., Schmoll, M., Kubicek, C. P., Ferreira, P., Ruiz-Dueñas, F. J., Martínez, A. T., Kersten, P. et al. (2009) Genome, transcriptome, and secretome analysis of wood decay fungus *Postia placenta* supports unique mechanisms of lignocellulose conversion. *Proc. Natl. Acad. Sci. U.S.A.* **106**, 1954–1959.
- Martínez, D., Larrondo, L. F., Putnam, N., Gelpke, M. D., Huang, K., Chapman, J., Helfenbein, K. G., Ramaiya, P., Detter, J. C., Larimer, F. et al. (2004) Genome sequence of the lignocellulose degrading fungus *Phanerochaete chrysosporium* strain RP78. *Nat. Biotechnol.* **22**, 695–700.
- Cullen, D. and Kersten, P. J. (2004) Enzymology and molecular biology of lignin degradation. In *Mycota III: Biochemistry and Molecular Biology* (Brambl, R. and Marzluf, G. A., eds), pp. 249–273. Springer, Berlin.
- Martínez, A. T., Speranza, M., Ruiz-Dueñas, F. J., Ferreira, P., Camarero, S., Guillén, F., Martínez, M. J., Gutiérrez, A. and del Río, J. C. (2005) Biodegradation of lignocelluloses: microbiological, chemical and enzymatic aspects of fungal attack to lignin. *Intern. Microbiol.* **8**, 195–204.

- 6 de Jong, E., Field, J. A. and de Bont, J. A. M. (1994) Aryl alcohols in the physiology of ligninolytic fungi. *FEMS Microbiol. Rev.* **13**, 153–188
- 7 Gallois, A., Gross, B., Langlois, D., Spinnler, H.-E. and Brunerie, P. (1990) Influence of culture conditions on production of flavour compounds by 29 ligninolytic basidiomycetes. *Mycol. Res.* **94**, 494–504
- 8 Ruiz-Dueñas, F. J. and Martínez, A. T. (2009) Microbial degradation of lignin: how a bulky recalcitrant polymer is efficiently recycled in nature and how we can take advantage of this. *Microbial Biotechnol.* **2**, 164–177
- 9 Gutiérrez, A., Caramelo, L., Prieto, A., Martínez, M. J. and Martínez, A. T. (1994) Anisaldehyde production and aryl-alcohol oxidase and dehydrogenase activities in ligninolytic fungi from the genus *Pleurotus*. *Appl. Environ. Microbiol.* **60**, 1783–1788
- 10 Guillén, F. and Evans, C. S. (1994) Anisaldehyde and veratraldehyde acting as redox cycling agents for H₂O₂ production by *Pleurotus eryngii*. *Appl. Environ. Microbiol.* **60**, 2811–2817
- 11 Guillén, F., Martínez, A. T. and Martínez, M. J. (1992) Substrate specificity and properties of the aryl-alcohol oxidase from the ligninolytic fungus *Pleurotus eryngii*. *Eur. J. Biochem.* **209**, 603–611
- 12 Varela, E., Martínez, M. J. and Martínez, A. T. (2000) Aryl-alcohol oxidase protein sequence: a comparison with glucose oxidase and other FAD oxidoreductases. *Biochim. Biophys. Acta* **1481**, 202–208
- 13 Varela, E., Martínez, A. T. and Martínez, M. J. (1999) Molecular cloning of aryl-alcohol oxidase from *Pleurotus eryngii*, an enzyme involved in lignin degradation. *Biochem. J.* **341**, 113–117
- 14 Ruiz-Dueñas, F. J., Ferreira, P., Martínez, M. J. and Martínez, A. T. (2006) *In vitro* activation, purification, and characterization of *Escherichia coli* expressed aryl-alcohol oxidase, a unique H₂O₂-producing enzyme. *Protein Expr. Purif.* **45**, 191–199
- 15 Varela, E., Guillén, F., Martínez, A. T. and Martínez, M. J. (2001) Expression of *Pleurotus eryngii* aryl-alcohol oxidase in *Aspergillus nidulans*: purification and characterization of the recombinant enzyme. *Biochim. Biophys. Acta* **1546**, 107–113
- 16 Fernández, I. S., Ruiz-Dueñas, F. J., Santillana, E., Ferreira, P., Martínez, M. J., Martínez, A. T. and Romero, A. (2009) Novel structural features in the GMC family of oxidoreductases revealed by the crystal structure of fungal aryl-alcohol oxidase. *Acta Crystallogr. D* **65**, 1196–1205
- 17 Ferreira, P., Hernández-Ortega, A., Herguedas, B., Martínez, A. T. and Medina, M. (2009) Aryl-alcohol oxidase involved in lignin degradation: a mechanistic study based on steady and pre-steady state kinetics and primary and solvent isotope effects with two different alcohol substrates. *J. Biol. Chem.* **284**, 2480–2487
- 18 Hassan-Abdallah, A., Bruckner, R. C., Zhao, G. H. and Jorns, M. S. (2005) Biosynthesis of covalently bound flavin: isolation and *in vitro* flavinylation of the monomeric sarcosine oxidase apoprotein. *Biochemistry* **44**, 6452–6462
- 19 Ferreira, P., Medina, M., Guillén, F., Martínez, M. J., van Berkel, W. J. H. and Martínez, A. T. (2005) Spectral and catalytic properties of aryl-alcohol oxidase, a fungal flavoenzyme acting on polyunsaturated alcohols. *Biochem. J.* **389**, 731–738
- 20 Wagner, M. A. and Jorns, M. S. (2000) Monomeric sarcosine oxidase. 2. Kinetic studies with sarcosine, alternate substrates, and a substrate analogue. *Biochemistry* **39**, 8825–8829
- 21 Gibson, Q. H., Swoboda, B. E. and Massey, V. (1964) Kinetics and mechanism of action of glucose oxidase. *J. Biol. Chem.* **239**, 3927–3934
- 22 Sancho, J. and Gómez-Moreno, C. (1991) Interaction of ferredoxin-NADP⁺ reductase from *Anabaena* with its substrates. *Arch. Biochem. Biophys.* **288**, 231–238
- 23 Medina, M., Martínez-Julvez, M., Hurley, J. K., Tollin, G. and Gómez-Moreno, C. (1998) Involvement of glutamic acid 301 in the catalytic mechanism of ferredoxin-NADP⁺ reductase from *Anabaena* PCC 7119. *Biochemistry* **37**, 2715–2728
- 24 Marchal, S. and Branlant, G. (1999) Evidence for the chemical activation of essential Cys-302 upon cofactor binding to nonphosphorylating glyceraldehyde 3-phosphate dehydrogenase from *Streptococcus mutans*. *Biochemistry* **38**, 12950–12958
- 25 Teng, H., Segura, E. and Grubmeyer, C. (1993) Conserved cysteine residues of histidinol dehydrogenase are not involved in catalysis: novel chemistry required for enzymatic aldehyde oxidation. *J. Biol. Chem.* **268**, 14182–14188
- 26 Olson, L. P., Luo, J., Almarsson, O. and Bruice, T. C. (1996) Mechanism of aldehyde oxidation catalyzed by horse liver alcohol dehydrogenase. *Biochemistry* **35**, 9782–9791
- 27 Garattini, E., Fratelli, M. and Terao, M. (2008) Mammalian aldehyde oxidases: genetics, evolution and biochemistry. *Cell. Mol. Life Sci.* **65**, 1019–1048
- 28 Corbier, C., Della, S. F. and Branlant, G. (1992) A new chemical mechanism catalyzed by a mutated aldehyde dehydrogenase. *Biochemistry* **31**, 12532–12535
- 29 Ge, X., Penney, L. C., van de Rijn, I. and Tanner, M. E. (2004) Active site residues and mechanism of UDP-glucose dehydrogenase. *Eur. J. Biochem.* **271**, 14–22
- 30 Fan, F., Germann, M. W. and Gadda, G. (2006) Mechanistic studies of choline oxidase with betaine aldehyde and its isosteric analogue 3,3-dimethylbutylaldehyde. *Biochemistry* **45**, 1979–1986
- 31 Eisses, K. T. (1989) On the oxidation of aldehydes by alcohol-dehydrogenase of *Drosophila melanogaster*: evidence for the *gem*-diol as the reacting substrate. *Bioorg. Chem.* **17**, 268–274
- 32 Ferreira, P., Ruiz-Dueñas, F. J., Martínez, M. J., van Berkel, W. J. H. and Martínez, A. T. (2006) Site-directed mutagenesis of selected residues at the active site of aryl-alcohol oxidase, an H₂O₂-producing ligninolytic enzyme. *FEBS J.* **273**, 4878–4888
- 33 Hernández, A., Ferreira, P., Martínez, M. J., Romero, A. and Martínez, A. T. (2008) Discriminating the role of His502 and His546 in the catalysis of aryl-alcohol oxidase. In *Flavins and Flavoproteins 2008: Proceedings of the Sixteenth International Symposium* (Fargo, S., Gomez-Moreno, C. and Medina, M., eds), pp. 303–308, Pressas Universitarias, Zaragoza
- 34 Fan, F. and Gadda, G. (2005) On the catalytic mechanism of choline oxidase. *J. Am. Chem. Soc.* **127**, 2067–2074
- 35 Gadda, G. (2008) Hydride transfer made easy in the reaction of alcohol oxidation catalyzed by flavin-dependent oxidases. *Biochemistry* **47**, 13745–13753
- 36 Winberg, J. O. and McKinley-McKee, J. S. (1998) *Drosophila melanogaster* alcohol dehydrogenase: mechanism of aldehyde oxidation and dismutation. *Biochem. J.* **329**, 561–570
- 37 Barbosa, J. A. R. G., Sivaraman, J., Li, Y. G., Larocque, R., Matte, A., Schrag, J. D. and Cygler, M. (2002) Mechanism of action and NAD⁺-binding mode revealed by the crystal structure of L-histidinol dehydrogenase. *Proc. Natl. Acad. Sci. U.S.A.* **99**, 1859–1864
- 38 Gadda, G. (2003) Kinetic mechanism of choline oxidase from *Arthrobacter globiformis*. *Biochim. Biophys. Acta* **1646**, 112–118
- 39 Guillén, F., Martínez, A. T., Martínez, M. J. and Evans, C. S. (1994) Hydrogen peroxide-producing system of *Pleurotus eryngii* involving the extracellular enzyme aryl-alcohol oxidase. *Appl. Microbiol. Biotechnol.* **41**, 465–470
- 40 Romero, E., Ferreira, P., Martínez, A. T. and Martínez, M. J. (2009) New oxidase from *Bjerkandera* arthroconidial anamorph that oxidizes both phenolic and nonphenolic benzyl alcohols. *Biochim. Biophys. Acta* **1794**, 689–697
- 41 de Jong, E., Field, J. A., Spinnler, H. E., Wijnberg, J. B. P. A. and de Bont, J. A. M. (1994) Significant biogenesis of chlorinated aromatics by fungi in natural environments. *Appl. Environ. Microbiol.* **60**, 264–270
- 42 de Jong, E., Field, J. A., Dings, J. A. F. M., Wijnberg, J. B. P. A. and de Bont, J. A. M. (1992) *De novo* biosynthesis of chlorinated aromatics by the white-rot fungus *Bjerkandera* sp. BOS55. Formation of 3-chloro-anisaldehyde from glucose. *FEBS Lett.* **305**, 220–224
- 43 Spinnler, H. E., de Jong, E., Mauvais, G., Semon, E. and Le Quééré, J.-L. (1994) Production of halogenated compounds by *Bjerkandera adusta*. *Appl. Microbiol. Biotechnol.* **42**, 212–221
- 44 de Jong, E. and Field, J. A. (1997) Sulfur tuft and turkey tail: biosynthesis and biodegradation of organohalogenes by basidiomycetes. *Annu. Rev. Microbiol.* **51**, 375–414
- 45 Thaller, V. and Turner, J. L. (1972) Natural acetylenes. XXXV. Polyacetylenic acid and benzenoid metabolites from cultures of the fungus *Lepista diemii* Singer. *J. Chem. Soc. Perkin Trans.* **1**, 2032–2034

Received 29 September 2009/29 October 2009; accepted 5 November 2009

Published as BJ Immediate Publication 5 November 2009, doi:10.1042/BJ20091499

SUPPLEMENTARY ONLINE DATA

Kinetic and chemical characterization of aldehyde oxidation by fungal aryl-alcohol oxidase

Patricia FERREIRA*†, Aitor HERNÁNDEZ-ORTEGA*, Beatriz HERGUEDAS†, Jorge RENCORET‡¹, Ana GUTIÉRREZ‡, María Jesús MARTÍNEZ*, Jesús JIMÉNEZ-BARBERO*, Milagros MEDINA†² and Ángel T. MARTÍNEZ*²

*Centro de Investigaciones Biológicas (CIB), Consejo Superior de Investigaciones Científicas (CSIC), Ramiro de Maeztu 9, E-28040 Madrid, Spain, †Departamento de Bioquímica y Biología Molecular y Celular, Facultad de Ciencias, and Instituto de Biocomputación y Física de Sistemas Complejos, Universidad de Zaragoza, E-50009 Zaragoza, Spain, and ‡Instituto de Recursos Naturales y Agrobiología de Sevilla (IRNAS), Consejo Superior de Investigaciones Científicas (CSIC), PO Box 1052, E-41080 Seville, Spain

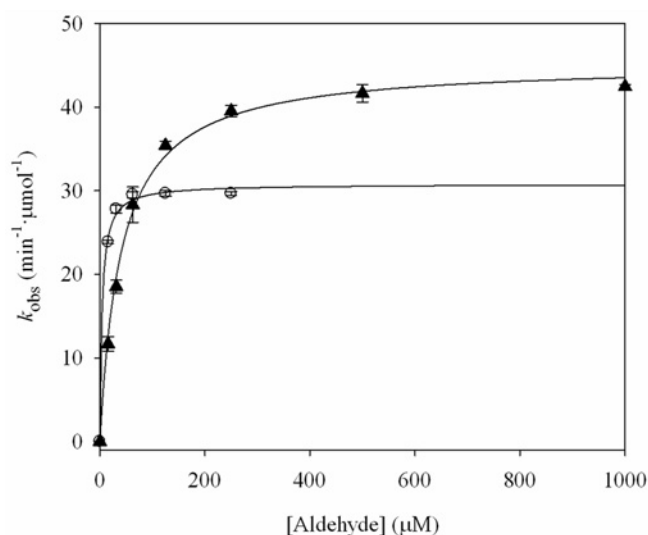


Figure S1 Kinetics of benzaldehyde and *p*-nitrobenzaldehyde oxidation by aldehyde dehydrogenase

Oxidation of benzaldehyde (▲) and *p*-nitrobenzaldehyde (○) by yeast aldehyde dehydrogenase was assayed by NADH formation in 0.1 M Tris/HCl, pH 8, containing 0.1 M KCl, 1 mM EDTA and 5 mM NAD⁺, at 25°C (k_{obs} , results are means \pm S.E.M.), and the benzaldehyde and *p*-nitrobenzaldehyde k_{cat} values ($45.3 \pm 0.8 \text{ min}^{-1}$ and $30.8 \pm 0.5 \text{ min}^{-1}$ respectively) were calculated.

¹ Present address: Great Lakes Bioenergy Research Center, University of Wisconsin–Madison, Madison, WI, U.S.A.

² Correspondence may be addressed to either of these authors (email mmedina@unizar.es or atmartinez@cib.csic.es)

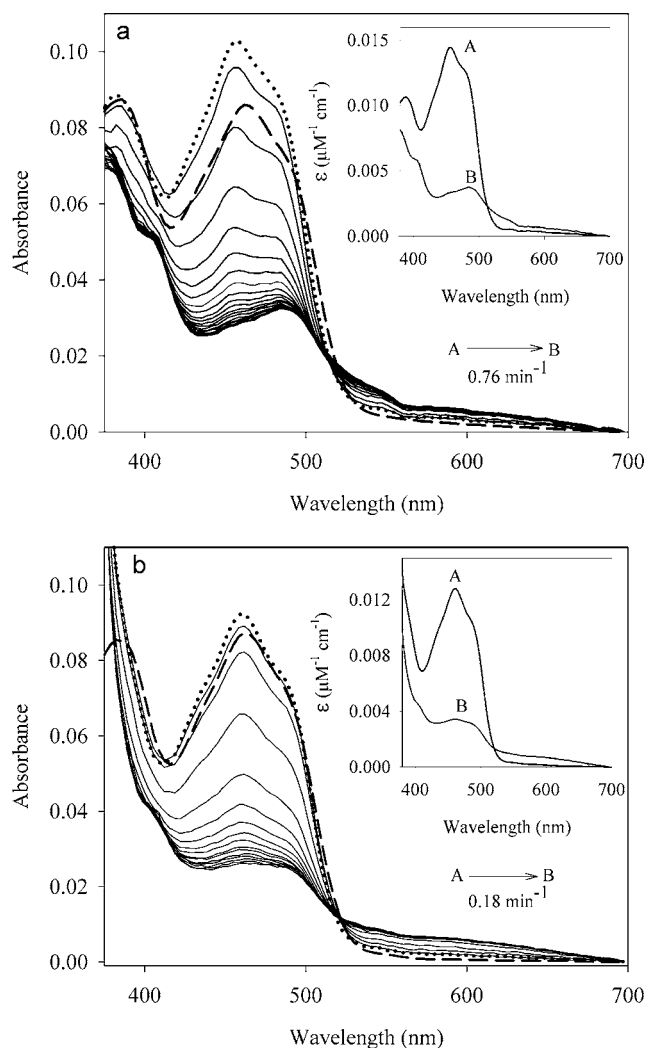


Figure S2 Spectral course of AAO anaerobic reduction with 3-chloro-*p*-anisaldehyde and veratraldehyde

AAO ($\sim 8 \mu\text{M}$) reduction with (a) 4.5 mM 3-chloro-*p*-anisaldehyde and (b) 2.5 mM veratraldehyde in 0.1 M sodium phosphate buffer, pH 6, at 24 °C was monitored using a diode-array stopped-flow spectrophotometer under anaerobic conditions. The initial AAO spectrum, and the first spectrum after mixing with the aldehydes are shown as (---) and (····) respectively. Spectra were recorded at different times after aldehyde addition: for (a) after 2.6 s, and then each 25 s for a total of 450 s; and for (b) after 10 s, and then each 200 s for a total of 3200 s. Insets show a deconvolution of the spectral changes during AAO reduction fitting to a two-step model ($A \rightarrow B$).

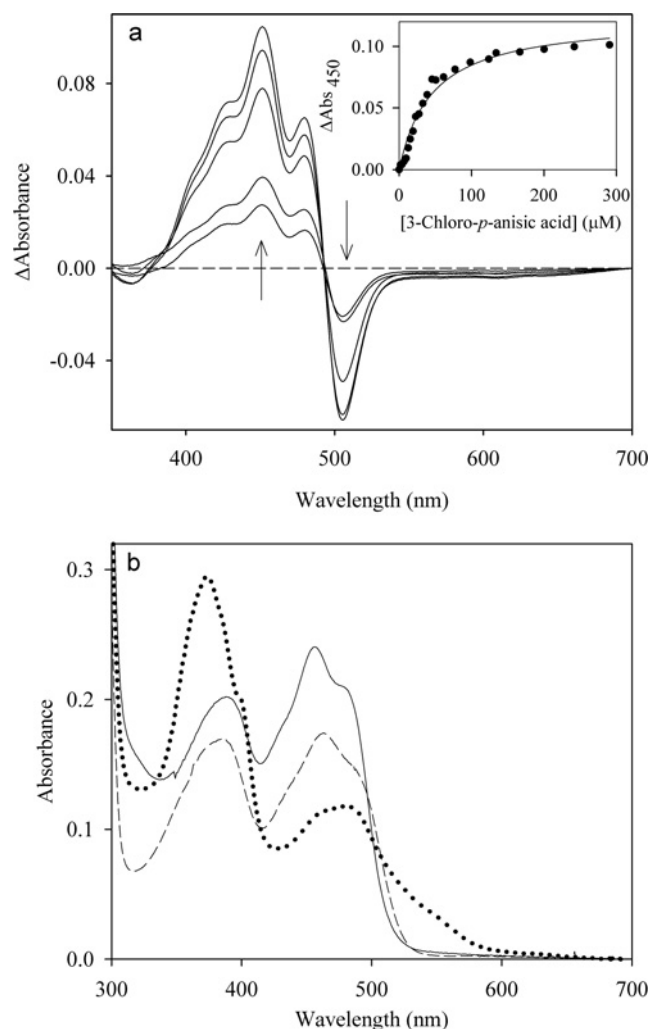


Figure S3 Acid titration of AAO and photoreduction of AAO-acid complex

(a) Difference spectra recorded during titration of 25 μM AAO with 19, 23, 77, 200 and 300 μM 3-chloro-*p*-anisaldehyde (in 0.1 M sodium phosphate buffer, pH 6, at 24 °C). The inset shows the observed increase in absorbance at 450 nm (●) plotted as a function of acid concentration, and a fit of the data to a theoretical binding curve (K_d of $45.5 \pm 5.2 \mu\text{M}$). (b) Photoreduction of the AAO complex with *p*-anisic acid. The curve (---) is the spectrum of oxidized AAO (16 μM) before titration. The solid curve is the spectrum of the AAO_{ox}-(*p*-anisic acid) complex obtained by adding a 356 μM concentration of the acid. The curve (····) is the spectrum of the AAO_{red}-(*p*-anisic acid) complex after photoreduction (in 0.1 M sodium phosphate buffer, pH 6, at 24 °C under anaerobic conditions in the presence of deazariboflavin).

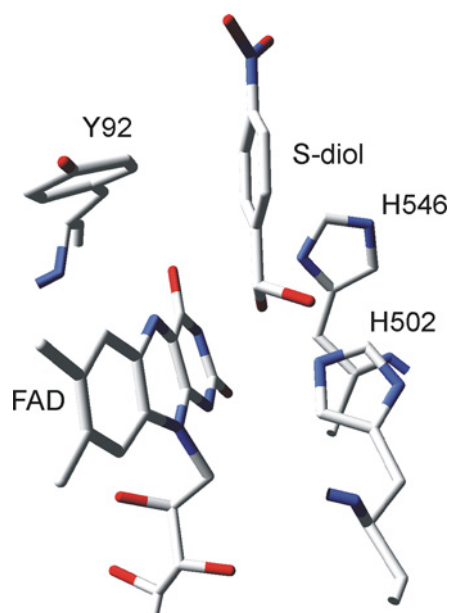


Figure S4 Location of active site His⁵⁰², His⁵⁴⁶ and Tyr⁹² in the AAO crystal structure

In the AAO crystal structure two histidine residues and one tyrosine residue are located at the active site, where a hydrated *p*-nitrobenzaldehyde molecule (S-diol) has been manually docked at the vicinity of the isoalloxazine ring of FAD. The His⁵⁰² and His⁵⁴⁶ side chains are at 2.5 Å and 3.2 Å (where 1 Å = 0.1 nm) distance respectively, from the *gem*-diol hydroxy group oxygens, whereas the isoalloxazine N5 and Tyr⁹² hydroxy group are at 3.0 Å and 6.3 Å respectively, from the α -carbon of the *gem*-diol. From PDB entry 3FIM.

Table S1 GC-MS analysis of acid formation during AAO oxidation of different aldehydes

The different acids formed after a 3 h incubation of 12 aldehydes with 0.3 μ M AAO were extracted, analysed by GC-MS without derivatization, and the oxidation rates estimated as molar percentages of the initial aldehyde concentration (1 mM or 4 mM). The main MS fragments are indicated, ordered by decreasing intensity. n/a, not available because no acid was formed.

Aldehyde	MS fragments (<i>m/z</i>)	Acid formed (%)
Benzoic acid	105, 122, 77, 51, 50	5
<i>p</i> -Anisic acid	135, 152, 77, 107, 92	17
Veratric acid	n/a	0
<i>m</i> -Chlorobenzoic acid	139, 156, 111, 75, 50	39
<i>p</i> -Chlorobenzoic acid	139, 156, 111, 75, 50	48
3-Chloro- <i>p</i> -anisic acid	186, 169, 115, 63, 77	2
<i>m</i> -Fluorobenzoic acid	123, 140, 95, 75, 50	5
<i>p</i> -Fluorobenzoic acid	123, 140, 95, 75, 50	20
3-4-Difluorobenzoic acid	141, 113, 158, 63, 93	7
<i>p</i> -Nitrobenzoic acid	65, 167, 109, 121, 150	43
2,4-Dinitrobenzoic acid	n/a	0
2,4-Hexadienoic acid	97, 67, 65, 95, 112	5

Table S2 NMR estimation of aldehyde hydration rates

The hydration rates of the different aldehydes assayed as AAO substrates were determined by integrating the peak areas of the benzylic protons of the diol [$\text{H}-\text{C}-(\text{OH})_2$] and aldehyde ($\text{H}-\text{C}=\text{O}$) species in ^1H -NMR spectra ($\text{H}_{\alpha'}$ and H_{α} respectively in Figure 4 of the main paper). The corresponding chemical shifts (δ_{H}) are also indicated.

Aldehyde	δ_{H} (p.p.m.)		Hydration rate (%)
	Diol	Aldehyde	
Benzaldehyde	5.97	9.86	1.0
<i>p</i> -Anisaldehyde	n/a	9.69	0
Veratraldehyde	n/a	9.66	0
<i>m</i> -Chlorobenzaldehyde	5.95	9.84	4.4
<i>p</i> -Chlorobenzaldehyde	5.96	9.84	1.0
3-Chloro- <i>p</i> -anisaldehyde	5.91	9.69	0.9
<i>m</i> -Fluorobenzaldehyde	5.96	9.86	3.0
<i>p</i> -Fluorobenzaldehyde	5.97	9.81	0.7
3-4-Difluorobenzaldehyde	5.94	9.79	3.1
<i>p</i> -Nitrobenzaldehyde	6.07	10.03	19.5
2,4-Dinitrobenzaldehyde	6.54	10.35	82.8
2,4-Hexadienal	5.73	9.31	0.4